Dynamic emissive signatures of intramolecular singlet fission during equilibration to steady state revealed from stochastic kinetic simulations

David J. Walwark, and John K. Grey

COLLECTIONS

Paper published as part of the special topic on Up- and Down-Conversion in Molecules and MaterialsUAD2020

View Online   Export Citation   CrossMark

ARTICLES YOU MAY BE INTERESTED IN

Vibronic coupling density analysis and quantum dynamics simulation for singlet fission in pentacene and its halogenated derivatives
The Journal of Chemical Physics 153, 134302 (2020); https://doi.org/10.1063/5.0024746

Charge transfer via spin flip configuration interaction: Benchmarks and application to singlet fission
The Journal of Chemical Physics 153, 064109 (2020); https://doi.org/10.1063/5.0018267

Singlet fission
The Journal of Chemical Physics 153, 110401 (2020); https://doi.org/10.1063/5.0026873
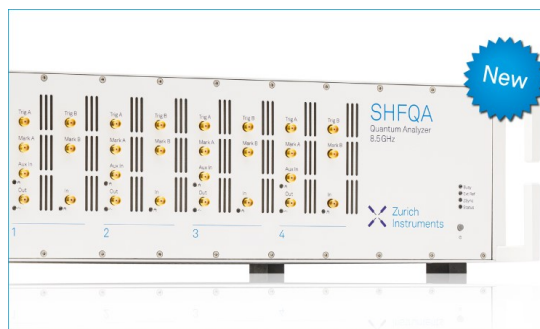
Dynamic emissive signatures of intramolecular singlet fission during equilibration to steady state revealed from stochastic kinetic simulations

View Online   Export Citation   CrossMark

David J. Walwark, Jr. (iD) and John K. Grey[a) (iD)

AFFILIATIONS

Department of Chemistry, University of New Mexico, Albuquerque, New Mexico 87131, USA

Note: This paper is part of the JCP Special Topic on Up- and Down-Conversion in Molecules and Materials.
[a)]Author to whom correspondence should be addressed: jkgrey@unm.edu

ABSTRACT

We investigate the ability of dynamic fluorescence probes to accurately track populations of multi-excitonic states in molecular dyads based on conjugated acenes capable of intramolecular singlet fission (iSF). Stochastic simulations of reported photophysical models from time-resolved spectroscopic studies of iSF dyads based on large acenes (e.g., tetracene and pentacene) are used to extrapolate population and fluorescence yield dynamics. The approach entails the use of repetitive rectangular-shaped excitation waveforms as a stimulus, with durations comparable to triplet lifetimes. We observe unique dynamics signatures that can be directly related to relaxation of multi-exciton states involved over the entire effective time of singlet fission in the presence and absence of an excitation light stimulus. In particular, time-dependent fluorescence yields display an abrupt decay followed by slower rise dynamics appearing as a prominent "dip" feature in responses. The initial fast decrease in the fluorescence yield arises from the formation of triplet pairs and separated triplets that do not produce emission resembling a complete ground state bleach effect. However, relaxation of one separated triplet allows the system to absorb, and in some cases, this increases the fluorescence yield, causing rise dynamics in the emissive response. Our approach also permits extrapolation of all multi-exciton state population dynamics up to steady state conditions in addition to the ability to explore consequences of alternative relaxation channels. The results demonstrate that it is possible to resolve unique signatures of singlet fission events from dynamic fluorescence studies, which can augment detection capabilities and extend sensitivity limits and accessible time scales.

Published under license by AIP Publishing. https://doi.org/10.1063/5.0027579

I. INTRODUCTION

Generating and harvesting multiple spin-forbidden excited states has promise for improving performance metrics of optoelectronic devices based on organic materials.[1–3] Singlet fission, where two triplet (S = 1) excitons are produced from a prompt singlet (S = 0) state almost immediately following photon absorption, has generated intense interest for enhancing photovoltaic performance in organic solar cells.[4–7] This multi-step mechanism first entails formation of a spinless triplet pair state (i.e., $[T–T]^1$), usually occurring on sub-ps time scales, followed by decohering into two separate triplets (i.e., T_1) on longer time scales.[4] The latter step effectively determines the overall triplet yield and has important

ramifications for utilizing triplets generated from singlet fission.[4] For example, the relatively long triplet lifetime implies a strong likelihood of significant triplet–triplet interactions in addition to interactions between triplets with other excitons and polarons of different spin and charge.[2,8,9] Triplets also tend to be more localized in nature, which has generated interest for preserving the $[T–T]$ state as long as possible. Ideally, triplets should be harvested rapidly (i.e., well before any potentially detrimental processes remove population density) although structural factors ranging from molecular conformation and packing to morphological considerations and device architecture impart significant challenges for achieving this goal in actual devices.[10–13] Resolving and understanding higher order interactions involving long-lived triplets is, therefore, important for not

only photovoltaics but other optoelectronic applications as well, such as upconversion processes seeking to exploit triplet–triplet annihilation leading to radiative emission from the higher energy singlet.[14–17]

Probing triplet processes on time scales comparable to their natural lifetimes can be difficult using conventional absorptive spectroscopic probes largely due to available sensitivities and, hence, concentration and excitation density requirements needed to obtain good signal-to-noise levels. However, there are few, if any, alternative spectroscopic probes of singlet fission and products on a wider range of time scales. Here, we propose a new strategy for capturing relaxation dynamics of population states involved in singlet fission in addition to triplet interactions on intermediate time scales (i.e., ~1 μs–1 ms) with high sensitivity. Fluorescence emission offers useful perspectives of triplets and other "dark" excited states and may be extended to single molecule level detection. We investigate the feasibility of fluorescence-based probes to interrogate multi-exciton relaxation dynamics in systems capable of undergoing intramolecular singlet fission (iSF).[18–23] Unlike traditional intermolecular singlet fission (xSF) materials (e.g., conjugated acene crystals), a much broader palette of iSF-active molecules is available, which may further be tailored to elicit desired packing motifs in the solid state.[24–29]

Because singlet fission requires a spinless excited state (i.e., S_1) adjacent to a chromophore in its ground electronic state (i.e., S_0), the simplest iSF system is achieved by covalently linking two chromophores (e.g., tetracene or pentacene derivatives) via a central moiety.[5,20,26,30,31] The current widespread interest in these iSF-active dyads as well as larger oligomers and polymers[18,23,25,27] has produced a rich body of literature concentrating on the early photophysics of singlet fission (i.e., $[T–T]^1$ formation and relaxation), which provides a useful basis for extrapolating triplet interactions on long time scales using fluorescence spectroscopy. Our approach involves using reported photodynamic models for a select group of iSF-active dyads, which are reformulated from a stochastic perspective, including explicit higher order processes. This method enables approximation-free evolution of the photodynamic model from a relaxed state to steady state under excitation by a stream of photons with explicit arrival times. We recently utilized a similar approach to demonstrate that the iSF activity can be detected from steady state fluorescence yields by varying excitation intensities (i.e., rates).[32] We now expand these capabilities to capture relaxation dynamics on μs time scales by simulating the underlying state population dynamics and the resultant emissive properties.

Excitation of individual iSF dyads is achieved by using rectangular (quasi-CW) excitation pulse waveforms that are averaged over many cycles (Excitation Intensity Modulation Spectroscopy or EIMS). Unique dynamics signatures emerge when iSF yields are appreciable, originating from the effect of triplet relaxation and re-excitation in the presence of a triplet when singlet fission is not possible. We then show how triplet lifetimes and population dynamics evolve both in the presence and absence of the excitation stimulus that can be used to validate contributions of specific states to the observed fluorescence dynamical features. The results demonstrate the potential value for extrapolating population state relaxation dynamics using fluorescence techniques that are also amenable to single molecule level investigations. Furthermore,

stochastic perspectives of multi-exciton processes offer deeper insights of iSF systems because the simulations are limited to a finite number of constituent chromophores comprising the dyad.

II. METHODS

A key challenge for utilizing fluorescence methods to detect singlet fission is the fact that emission yields tend to be low (<1%) for either iSF or xSF systems.[31,33–35] However, in a recent study, we found that large fluctuations in steady state fluorescence intensities occur in single iSF dyads when varying excitation rates over several decades.[32] Specifically, large increases in fluorescence yields appear with increasing excitation intensity (rates) due to the larger emission yields of triplet-containing absorbing states (i.e., $S_0 T_1$), even when accounting for a diminished absorption cross section (assuming triplets do not absorb and, therefore, do not contribute to the fluorescence signal). Increasing the excitation intensity further results in population saturation of presumed non-absorptive states in iSF dyads (i.e., $T_1 T_1$ and $S_1 T_1$) and reduced excitation (and thus emission) yields. Fortunately, fluorescence detection of triplets and their relaxation and interaction dynamics have been studied extensively in organic systems, especially at the single molecule level, which is still possible even in systems with very low yields (e.g., <1%).[36–40] Stochastic behaviors may also be resolved making the extension of fluorescence emission particularly attractive for singlet fission detection that is achieved using EIMS to expose triplet interactions and relaxation dynamics. This hybrid technique involves repetitive excitation and synchronous averaging of rectangular-shaped laser pulses that is sensitive to the presence of dynamic quenchers, namely, triplets, which also reveals their population dynamics on time scales spanning ~100 ns to ~1 s.[37,41–43] EIMS has seen considerable use in the study of triplets in multi-chromophoric conjugated polymers where fluorescence dynamics responses display a wide range of behaviors depending on conformation and packing dependent exciton relaxation and spin conversion processes.[44] Although previous EIMS studies of polymers have demonstrated the likelihood of more than one triplet present at any time, singlet fission was never considered as a triplet-generating mechanism because of the extreme variability of accessible photophysical channels in polymers depending on conformational and packing qualities.

We investigate model dyad systems known to undergo iSF by performing stochastic kinetic simulations of EIMS experiments on time scales comparable to the natural triplet lifetime. It is helpful to stress that our present application is limited to fluorescence dynamics on ~1 μs–1 ms time scales that, while not directly probing early SF processes, is particularly sensitive to triplet relaxation dynamics because these processes are confined to single iSF-active dyads. Photophysical models of iSF dyads were adapted from Refs. 19, 26, and 45–47 consisting of substituted pentacene and tetracene derivatives covalently tethered to a non-conjugated core moiety. Dyad conformational qualities are largely dictated by the core geometry and bonding motif, which also govern electronic coupling between the pendant acene chromophores.[24] For simplicity, we assume that only weak interchromophore coupling exists, thereby enabling the use of well-defined spin states (i.e., S_0, S_1, T_1). Structures of the iSF dyads are depicted in Scheme 1.
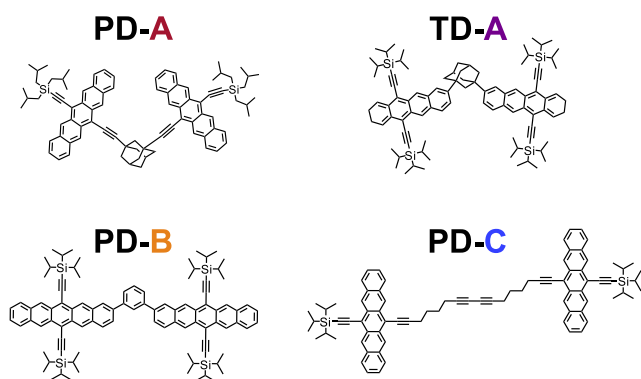
SCHEME 1. Molecular structures of iSF dyads (see Table I for specific photophysical constants, *vide infra*).

We then adapted photophysical models reported with each iSF dyad, which are outlined in Scheme 2, and the corresponding photophysical constants appear in Table I. Additionally, these models originally solved all coupled rate equations deterministically entailing formulating all bimolecular reactions as pseudo-first order processes. While all models include singlet fission as well as triplet pair spin conversion, relaxation channels vary slightly depending on the specific physical probes employed in each study.

Our basic approach entails reformulating these models from a purely stochastic perspective that not only preserves the source model kinetics faithfully but also explicitly uses the specific reaction stoichiometry and molecularity (i.e., bimolecular reactions). Moreover, stochastic solutions are approximation-free allowing for extrapolation of state populations and reaction yields (i.e., fluorescence) up to steady state levels with no accumulated numerical error. Because details of the stochastic approach were discussed at length earlier,[32] we limit our description to the specific application at hand, namely, excitation and relaxation dynamics on sub-ms time scales. Our selection of iSF-active systems also span a broad range of reported singlet fission yields in order to better highlight the ability of fluorescence-based probes to report on the relaxation of triplet-containing multi-exciton states originating from singlet fission.

Our simulation algorithm is based on the modified next reaction method,[48] and reaction stoichiometries are set by the specific model reported for each iSF dyad. We did include the possibility of intersystem crossing via the usual perturbative mechanism even if it was not included in the original model, which is only a minority triplet-producing channel in all pentacene dyad (PD) cases. Because of the range of relaxation channels, the simulation must perform many realizations in order to accurately calculate state populations and reaction yields. In contrast to our earlier study,[32] where the excitation rate constant (k_{exc}) was varied and the reaction progress was sampled near equilibration to obtain steady state levels of populations and yields, the simulations herein differ, in that k_{exc} remains constant, while the excitation stimulus is on.
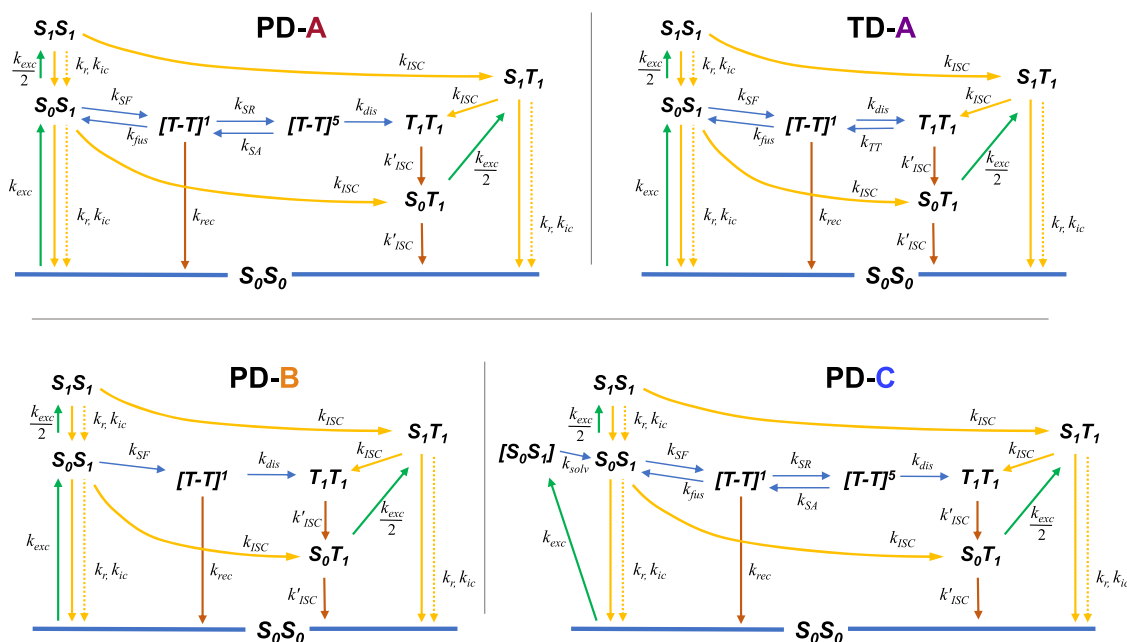
SCHEME 2. Photophysical models for each iSF dyad adapted from Refs. 19, 26, and 45–47. Processes added in the stochastic version are denoted by gold lines. Note: All processes are depicted as unimolecular following original literature sources although our simulations treated bimolecular reactions explicitly. Only TD-A included the possibility of triplet–triplet annihilation (k_{TT}), and we did not add this channel to the other models.

TABLE I. Parameters from iSF dyad photophysical models.

Process	Rate constant (s^{-1})	Dyad			
		PD-A[a]	PD-B[b]	PD-C[c]	TD-A[d]
Singlet fission	k_{SF}	2.4×10^9	2.1×10^9	1.4×10^8	1.5×10^8
Triplet pair fusion	k_{fus}	5×10^7	...	1.4×10^7	1.3×10^7
Singlet relaxation[e]	k_{S_1}	9.5×10^7	6.5×10^7	1.9×10^8	8.7×10^7
Triplet pair recombination (S_0S_0)	k_{rec}	1×10^7	2.6×10^6	4.6×10^7	1.7×10^7
Triplet pair dissociation	k_{dis}	5.7×10^6	3.3×10^6	2.9×10^6	7.4×10^7
Reverse intersystem crossing	k'_{ISC}	3.12×10^4	5×10^4	3.4×10^4	5.7×10^3
Triplet pair quintet formation	k_{SR}	1.1×10^7	...	1.2×10^8	...
Triplet pair singlet recombination	k_{SA}	4.8×10^6	...	3.6×10^6	...
Solvation	k_{solv}	...	...	5.5×10^{10}	...
Triplet–triplet annihilation	k_{TT}	...	...	...	1.1×10^7
Internal conversion	k_{ic}	4×10^7	1×10^7	1.35×10^8	7×10^6
Radiative emission	k_r	5.36×10^7	5.36×10^7	5.36×10^7	6.3×10^7
Intersystem crossing	k_{ISC}	1.43×10^6	1.43×10^6	1.43×10^6	1.7×10^7
Singlet reformation emission factor	β (%)	6.0	0	2.1	15.8
$\frac{\Phi_r(S_0T_1) \cdot \Phi_{exc}(S_0T_1)}{\Phi_r(S_0S_0)}$	...[f]	3.55	16.55	0.82	0.99

[a]Reference 47.
[b]Reference 26.
[c]Reference 45.
[d]Reference 46.
[e]$k_{S1} = k_r + k_{ic} + k_{ISC}$.
[f]$\Phi_{exc}(S_0T_1) \equiv \frac{1}{2}$.

A. Simulating responses of monomers in the absence of singlet fission

It is first instructive to consider the simplest possible system (i.e., in the absence of any higher order relaxation channels) using our stochastic method. A significant advantage of stochastic simulations on an analytically solvable system is that it produces results in the same form as experiment (i.e., emission counts binned in ~100 ns bins) and, if desired, with similar noise levels. Figure 1(a) displays a typical rectangular excitation pulse waveform used to excite fluorescence in a TIPS-pentacene molecule. Throughout this work, we employ similar idealized rectangular shaped pulses for all simulations with no rise time (see the supplementary material for details of numeric pulse generation). Because many reported iSF-active dyads and larger systems employ TIPS-pentacene as their constituent chromophores,[19,20,23,49–51] we adapt this molecule as a benchmark "monomer" system. The sparse nature of excited density of states further enables the use of a simple three-level system consisting of the ground and excited state singlets (i.e., S_0 and S_1) and the lowest energy triplet (i.e., T_1). For a more detailed discussion of this particular problem and its implications on single molecule photophysics through EIMS, see Ref. 43.

Figure 1(b) shows a simulated EIMS response from a single TIPS-pentacene monomer generated for $k_{exc} = 10^7$ s^{-1}. From the experimental perspective, once the excitation waveform turns on, the system has a non-zero probability of transitioning to the emissive S_1 state and the fluorescence intensity begins at an initial value, I_0. As time progresses, there is an increasing likelihood of occupying a triplet causing intensity to decay to a steady state level, I_{ss}, due to triplet population dynamics.[43] Triplet yields (Φ_{ISC}) typically vary considerably for TIPS-pentacene, and we used a conservative estimate of 1.43×10^6 s^{-1} for the intersystem crossing rate constant, k_{ISC}, resulting in a value of 2% for Φ_{ISC}. While various neutral and charged states may also quench fluorescence,[39] the dynamic quenching modulation behavior in EIMS responses arises solely from triplets that can be easily confirmed experimentally by performing measurements under different environments.

The simple monomer simulation in Fig. 1 provides a useful basis for interpreting responses from dyads (vide infra) since only unimolecular triplet processes are possible. Fluorescence modulation occurs from the non-zero probability that the monomer will transition to a triplet, which can be directly assessed from the contrast ratio using experimentally measured I_0/I_{ss} values. Here, it is more convenient to write these observables in terms of the steady state S_0 probability, which is a direct result of this experiment [i.e., $\mathrm{Prob}(S_0, ss) = I_{ss}/I_0$], and by assuming $\mathrm{Prob}(S_1)$ is small, the steady state triplet population can also be inferred from fluorescence intensities: $\mathrm{Prob}(T_1, ss) \approx \left(1 - \frac{I_{ss}}{I_0}\right)$. Because the present work emphasizes simulations of EIMS responses and state population dynamics, we use the theoretical fluorescence yield, Φ_r, to describe the triplet-induced fluorescence intensity modulation. This quantity not only changes as a function excitation intensity but also with time [$\Phi_r(k_{exc}, t)$], until settling into the steady state emission yield, denoted by $\Phi_r(k_{exc}, ss)$.
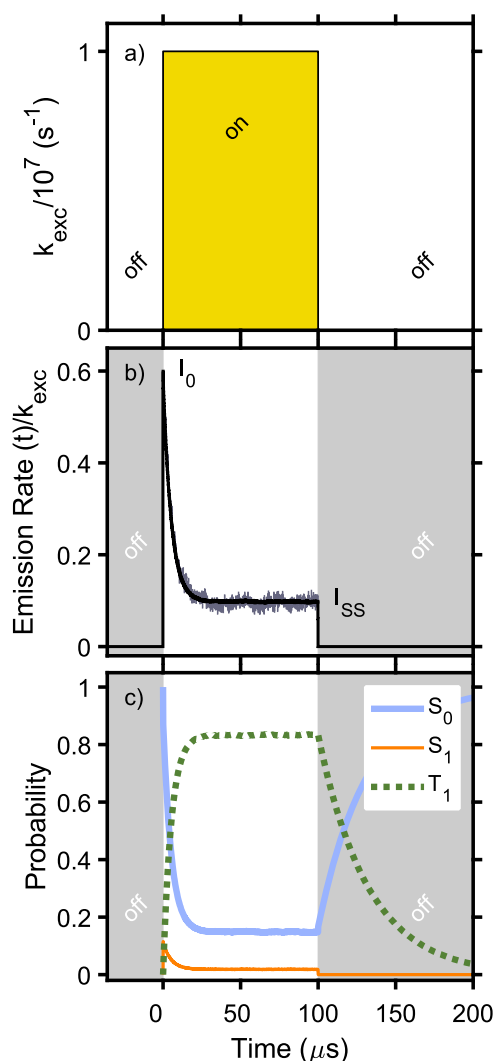
FIG. 1. TIPS-pentacene monomer model. (a) Idealized rectangular excitation pulse. (b) Simulated emissive (EIMS) response, averaged over 1200 (gray) or 120 000 (black) repetitions. Each simulated experiment takes 500 μs for one repetition corresponding to total times of 60 s (gray) of observation time, assuming a 1% collection efficiency. The black trace represents acquiring for 6000 s or over 60 s at 100% detection efficiency. (c) Probabilities of relevant species. At this excitation rate (10^7 s^{-1}), the steady state S_1 occupation is 1.9%, S_0 is 14.7%, and T_1 is 83.4%.

Population dynamics of each species are shown in Fig. 1(c) where it can be readily seen that the monomer system spends most of its time in the S_0 and T_1 states, as expected.[44] Population loss (buildup) dynamics of S_0 (T_1) recover (decay) after the excitation light is turned off. Additional perspectives on triplet quenching and extension to multi-chromophoric molecules have been discussed in detail in Refs. 43 and 44. Systems lacking appreciable excitonic interactions will appear identical to the monomer

case, with a monotonically decreasing emissive response to a square excitation pulse.

B. Extending the model to iSF dyads: Bimolecular relaxation channels

Beginning with the three-level photophysical rate equations, addition of another chromophore (as realized in iSF dyads) mainly entails the need to include bimolecular processes and multi-exciton states. While this study focuses on multi-triplet generation via iSF, other bimolecular decay mechanisms may become important, such as exciton–exciton annihilation. However, we limit the scope of the study to only specific reactions provided in the original models (*vide infra*), but additional studies are provided in the supplementary material that investigate the effects of varying triplet formation and relaxation. Scheme 1 depicts the molecular structures of selected iSF dyads adapted from literature sources.

We denote these iSF systems as TD (tetracene dyad) and PD (pentacene dyad) molecules, respectively, followed by a letter (e.g., PD-A and PD-B), and the corresponding photophysical constants from each source are provided in Table I. Scheme 2 next depicts the photophysical models in graphic form for each iSF dyad in this study, including the excitation of possible absorbing states.

Although our adaptation did not modify original decay channels, we did include the possibility for intersystem crossing as well as radiative and non-radiative relaxation even if these explicit processes did not appear in the original source. We estimated these quantities from related systems,[52,53] and we assume the same rate constants (i.e., k_{ISC} and k_r) for all iSF dyads. The only exception being the TD-A system in which all rate constants used in our simulations were included in the original model. Furthermore, the rate constant for non-radiative singlet relaxation, k_{IC}, was allowed to vary, but the known singlet lifetimes were preserved. Because the models differ slightly between iSF dyads (see Table I), we use each specific form and implement the stochastic simulation algorithm to generate exact realizations of the system evolution in time, but the basic assumptions of our computational approach are the same.[54] The simulations were also strictly zero-dimensional, thereby neglecting any molecular geometry or chromophore orientation considerations.

Initially, all systems reside in the ground electronic state (denoted here as S_0S_0), the primary absorbing state. Single photon excitation results in one excited singlet (S_0S_1), and singlet fission follows the same reaction stoichiometry as originally formulated where S_0S_1 decays into a correlated triplet pair state ($[T–T]$). In some models (i.e., PD-A and PD-C), transitions between the singlet and quintet $[T–T]$ states are considered, whereas others (i.e., PD-B and TD-A) do not include this possibility. Nonetheless, all triplet pairs may decohere into two triplets (T_1T_1) and the dyad cannot absorb another photon, while either $[T–T]$ or T_1T_1 states are occupied, which leads to an effect resembling a ground state bleach. Only when a separated triplet relaxes (e.g., resulting in the S_0T_1 state), will the system be able to interact again with the excitation field. To this end, our model assumes that the state S_0T_1 may undergo photoexcitation to S_1T_1, but singlet fission is not possible that may be invalid in certain circumstances (e.g., when significant interchromophore coupling or charge transfer character exists).[5,55–57] Because only one chromophore site may be excited

at a time, the excitation yield for S_0T_1 is expected to be smaller than that of S_0S_0, which we assume is half since only one singlet ground state is present [i.e., $\Phi_{exc}(S_0T_1) \equiv \Phi_{exc}(S_0S_0)/2$]. Furthermore, these conditions dictate that only the S_0S_0 absorbing state is capable of undergoing singlet fission, and this principle underlies all the predictions herein. We also assume the lack of excited state absorption transitions (e.g., $S_1 \rightarrow S_n$ or $T_1 \rightarrow T_n$). This assumption generally holds when excitation rates are small, in addition to ensuring excitation energies are not resonant with $T_1 \rightarrow T_n$ transitions. Similarly, the rare and short-lived nature of the S_1S_1 state (while possible in our simulations) makes the likelihood of singlet–singlet annihilation exceptionally small, so the process is not considered further.

With these basic assumptions defined, models for each iSF dyad in Scheme 2 and Table I are solved stochastically using the exact number of chromophores (i.e., $N_c = 2$), thus enabling an explicit bimolecular formulation for the iSF reaction. We gain additional fidelity by including diminished excitation yields of S_0T_1 and S_0S_1 and allowing the complete stochastic effect of random fluctuations (e.g., S_0T_1 may or may not absorb excitation; the average chance is 50%) to contribute to fluorescence yields and state population dynamics.

Along similar lines, it is apparent from Fig. 1(c) that triplet populations relax for significantly longer times once the rectangular excitation waveform shuts off. We previously introduced a hybrid EIMS technique where two rectangular excitation pulses of the same intensity are temporally delayed by varying amounts, thereby sampling non-steady state triplet population dynamics.[40,42] The first pulse generates a steady state triplet population, which is verified by using a sufficiently long duration before it turns off. The second pulse then re-excites the system, and if the delay is shorter than the triplet lifetime, it is possible to estimate triplet relaxation time scales using the initial intensities (I_0) as an indicator for the presence of unrelaxed triplets. This variable rest delay variant of EIMS (i.e., VR-EIMS) has significant advantages over absorptive probes for estimating triplet lifetimes mainly from the fact that it yields the highest sensitivity when performed on single molecules. Moreover, this feature also makes VR-EIMS particularly amenable to stochastic simulations, which we exploit herein to further explore unrelaxed multi-exciton states. Specifically, we seek to further understand the possible roles of the S_0T_1 state in iSF dyads and assess if characteristic markers exist, which either confirm or disconfirm whether this state may form another triplet pair state if excited before the residual triplet decays completely. We now show in the following that unique and unambiguous signatures of singlet fission can be discerned from EIMS simulations of iSF-active dyads.

III. RESULTS AND DISCUSSION

A. On the fundamentals of the EIMS response in iSF dyads

In the following, we simulate EIMS responses of iSF-active dyads highlighted above using a rectangular excitation function waveform for several excitation intensities (rates). Pulse durations were selected such that the important dynamics are illustrated,

but steady state conditions are not reached in all cases. The non-zero probability of singlet fission of the prompt excitation into two triplets implies greater quenching efficacies due to significant ground state bleach, as outlined in Sec. II, but the temporary nature of this condition leads to distinctive signatures as the system relaxes to steady state levels.

Figure 2 shows EIMS responses from the four iSF dyads highlighted earlier in Table I and Scheme 2. Similar to Fig. 1, the "off" periods are denoted by gray bars when the system cannot be excited and the "on" period has a white background. These curves represent the time-dependent emission generated from the repetitive excitation of the rectangular pulse waveform for many cycles (viz. realizations), normalized by the excitation rate. Though not necessarily depicted, in a real experiment, long "off" times would follow the "on" period to allow complete relaxation of all triplet states prior to the next excitation cycle. In our simulations, we merely reset the system to a relaxed state before beginning the next realization. We then vary k_{exc} for the excitation pulse waveform according to predicted trends of the initial and steady state emission yields [i.e., $\Phi_r(S_0S_0)$ and $\Phi_r(k_{exc}, ss)$, respectively]. The modulation contrast and behaviors of responses likewise vary depending on the relative sizes of $\Phi_r(S_0S_0)$ and $\Phi_r(S_0T_1)$ and the probability of S_0T_1. Briefly, singlet fission effects on steady state fluorescence vary significantly with k_{exc} where an initial increase in the emission yield is often seen with increasing k_{exc} followed by a decrease due to saturation.[32]

Because of the more complicated nature of iSF dyad photophysics, it is first useful to define key terms and their impact on the fluorescence observable. The radiative yield of the relaxed system, *excluding delayed emission from singlet reformation*, is $\Phi_r(S_0S_0, rates)$. Explicitly, this "prompt" emission yield is given by $\Phi_r(S_0S_0, rates) = \frac{k_r}{k_r + k_{ic} + k_{isc} + k_{SF}}$, whereas the radiative yield of the S_0S_0 absorbing state that includes delayed emission, $\Phi_r(S_0S_0)$, has no brief mathematical definition. In summary, $\Phi_r(S_0S_0, rates)$ is the probability that S_0S_1 emits (and is relevant each time S_0S_1 is formed), whereas $\Phi_r(S_0S_0)$ is the probability that emission *eventually* results after excitation of S_0S_0 and is equivalent to Φ_r from an absolute emission quantum yield experiment. In PD-B, where iSF is irreversible, $\Phi_r(S_0S_0) = \Phi_r(S_0S_0, rates)$; in all other dyads, $\Phi_r(S_0S_0) > \Phi_r(S_0S_0, rates)$ due to delayed emission (see β in Table I). In the interest of completeness, we define $\Phi_{SF}(S_0S_0)$ as the probability that a triplet pair state that does not reform into S_0S_1 eventually results after excitation of S_0S_0; in all dyads besides PD-B, $\Phi_{SF}(S_0S_0) < \Phi_{SF}(S_0S_0, rates)$ due to singlet reformation.

During an EIMS experiment at a particular (non-saturative) excitation rate k_{exc}, emission yields of the dyads begin at $\Phi_r(S_0S_0, rates)$ and evolve in time [$\Phi_r(k_{exc}, t)$] due to the occupation of other states besides S_0S_0, and as contributions from delayed emission manifest. Depending on the average time of singlet reformation, delayed emission gradually adds to the emission yield, while increasing ground state bleach reduces the excitation yield. Eventually the system reaches a steady state emission yield [i.e., $\Phi_r(k_{exc}, ss)$] that may be larger than $\Phi_r(S_0S_0)$ in some cases (PD-A and PD-B): a complete reversal of the monomer behavior. Though this broad outline of the time-dependent emission yield is applicable to all the dyads studied here, differences in kinetic scheme and rate constants imply further details requiring consideration of the individual systems one at a time.
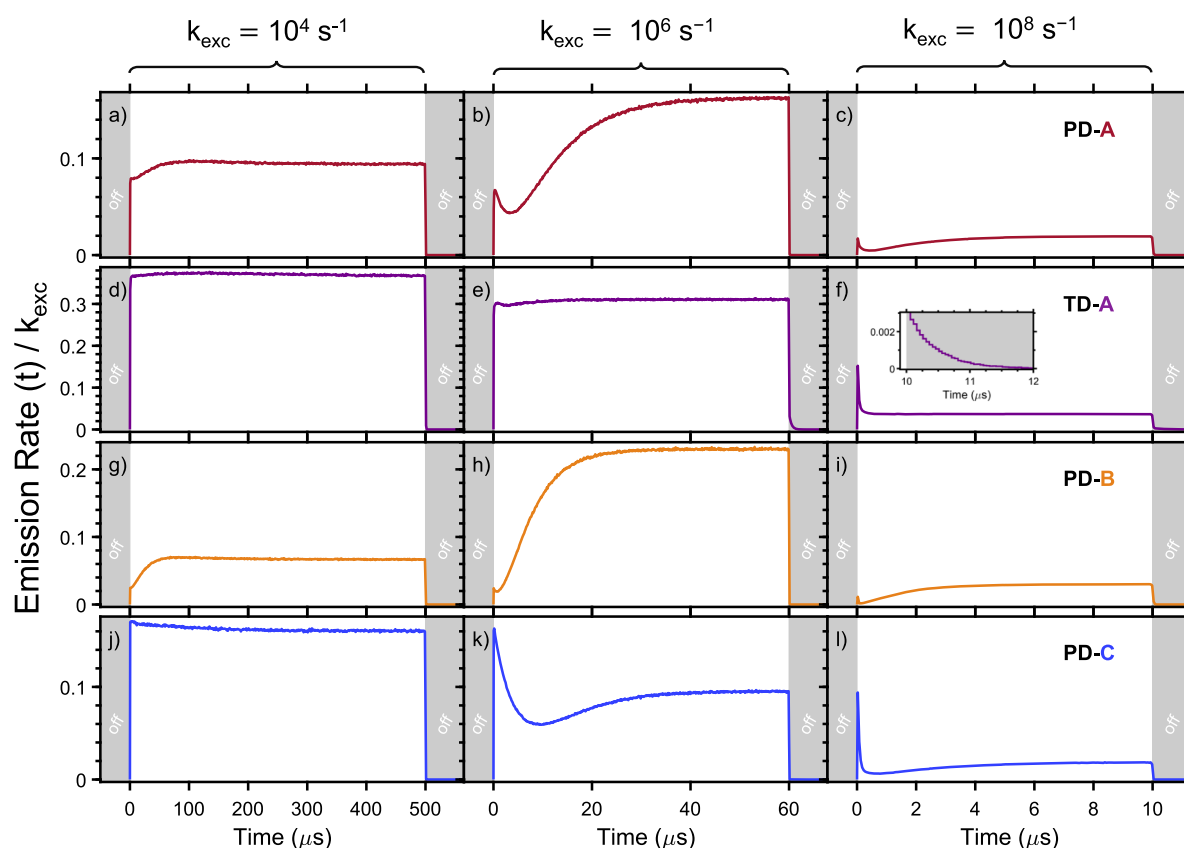
FIG. 2. Simulated EIMS responses displayed as emission rates normalized by the excitation rate for each dyad system (see Table I). The presence of the excitation pulse is indicated by a white background. Three different excitation regimes were investigated: low (k_{exc} = 10^4 s^{-1}, ~5 possible excitations per cycle, left column), intermediate (k_{exc} = 10^6 s^{-1}, ~60 possible excitations per cycle, middle column), and high (k_{exc} = 10^8 s^{-1}, ~1000 possible excitations per cycle, right column) for PD-A (a)–(c), TD-A (d)–(f), PD-B (g)–(i), and PD-C (j)–(l), respectively. Inset: The enlarged region of TD-A EIMS depicting delayed fluorescence following turn-off of the excitation waveform.

Perhaps the most surprising feature from these simulations is a transient regime with lower emission yields than either the initial response or the steady state level that gains prominence with increasing k_{exc} values. This "dip" in $\Phi_r(k_{exc}, t)$ is mainly a consequence of our assumption that both $[T{-}T]$ and T_1T_1 do not absorb nor emit. If a path exists for these singlet fission products to reform an emissive singlet, such as in the tetracene dyad model (see TD-A in Table I), then the emission dip is almost completely absent.

Beginning with the lowest excitation rate (k_{exc} = 10^4 s^{-1}; left column of Fig. 2), we see that $\Phi_r(k_{exc}, t)$ exhibits relatively little modulation although the productive [i.e., relatively high $\Phi_{SF}(S_0S_0)$] pentacene-based iSF dyads [PD-A, Fig. 2(a) and PD-B, Fig. 2(g)] show a slight rise in the yield on time scales of ~20 μs–50 μs due to non-zero Prob(S_0T_1) (*vide infra*). While the overall modulation depth is small, the rise dynamics qualitatively reflect ground state recovery dynamics due to relaxation of a triplet following $[T{-}T]$ dissociation. However, the recovery of ground states *per se* cannot increase the emission yield beyond $\Phi_r(S_0S_0)$. Instead, the greater emission yield of the S_0T_1 absorbing state is largely responsible for

observed fluorescence gains due to inactivation of the iSF channel. For the low iSF-yield pentacene dyad PD-C [Fig. 2(j)], the EIMS response is similar to the monomer in Fig. 1, with smaller emission yields at steady state. It is also interesting to note that the tetracene-based iSF dyad [TD-A, Fig. 2(d)] shows virtually no modulation of fluorescence, which is consistent with the fact that the emission yield of S_0T_1 is roughly twice that of S_0S_0. At this low excitation rate (five excitations per pulse cycle on average), delayed emission in TD-A is not observed because $k_{TT} \gg k_{exc}$.

Increasing the excitation intensity to k_{exc} = 10^6 s^{-1} (middle column of Fig. 2) reveals a more conspicuous effect on EIMS responses, especially those with large $\Phi_{SF}(S_0S_0)$ values [i.e., Figs. 2(b) and 2(h)]. To highlight the large change in time-dependent emission yields, each row of Fig. 2 shares a common y-axis scale. $\Phi_r(k_{exc}, t)$ shows a characteristic decrease immediately following turn-on of the excitation stimulus, common in all triplet modulation fluorescence quenching, which then experiences an abrupt turnaround with a prominent rise dynamical feature resulting in larger values of $\Phi_r(k_{exc}, ss)$. The prominent "dip" feature reflects the ground

state bleach effect mentioned earlier becoming accentuated with larger excitation frequencies and is always strongest in systems of even-parity in the chromophore number (i.e., N_c = 2, 4, 6). The large positive modulation in PD-A and PD-B indicates a higher probability of emission from the $S_0 T_1$ absorbing state.

The PD-C system exhibits the only response where later gains in $\Phi_r(k_{exc}, ss)$ following the initial decay do not overwhelm $\Phi_r(S_0 S_0)$ levels as time progresses. Yet, it demonstrates a clear dip indicating both chromophores are no longer able to absorb excitation light due to occupying triplet-containing states and, thus, temporarily have an emission yield of zero. Importantly, no other process is known to cause coherent ground state bleach besides iSF (not even singlet-triplet annihilation),[43] so we propose that the dip feature in the EIMS response is an unambiguous reporter of iSF. Only when triplet–triplet annihilation is appreciable, will this signature be diminished, such as in the case of TD-A, as evidenced by the very weak dip present in Fig. 2(e) due to a k_{TT} of 1.1×10^7 s^{-1} (accounting for N_c = 2). Additionally, large triplet yields from intersystem crossing may attenuate these characteristic responses of iSF (see the supplementary material), as well as larger numbers of constituent chromophores ($N_c > 2$). Interestingly, TD-A also shows a small but clearly resolved, delayed emission component once the excitation pulse terminates (see the inset of Fig. 2). This feature originates from triplet–triplet annihilation defined by the source model as the rate at which separated triplets reform a triplet pair (i.e., $T_1 + T_1 \rightarrow [T–T]$). Even though triplet–triplet annihilation obscures EIMS signatures of iSF, the evidence of this process may appear directly in fluorescence yields when the excitation waveform turns off. The lack of this channel in pentacene-based systems does not preclude the possibility of slow triplet–triplet annihilation and weak delayed fluorescence, which may be amended following further experimental studies. The behaviors presented here reflect unambiguous EIMS signatures of singlet fission: a "dip" due to occupation of $T_1 T_1$; higher emission yields at steady state in PD-A and PD-B (i.e., more productive iSF systems) at k_{exc} = 10^6 s^{-1} [Figs. 2(b) and 2(h)] in comparison to when k_{exc} = 10^4 s^{-1} [Figs. 2(a) and 2(g)].

At the highest excitation rate (k_{exc} = 10^8 s^{-1}, 1000 excitations per pulse cycle), overall fluorescence yields decrease substantially as singlet fission-induced modulation behaviors operate under a saturative regime. By comparison, TD-A, which also has the smallest average singlet fission yield, showed relatively small modulation at lower excitation rates [see Figs. 2(d) and 2(e)]. However, this behavior abruptly changes where $\Phi_r(k_{exc}, t)$ decays rapidly (i.e., <1 μs) to its steady state level, $\Phi_r(k_{exc}, ss)$. It is useful to point out that this type of EIMS response is more characteristic of rapid triplet formation and population decay often found in other multi-chromophoric systems (e.g., chalcogen-containing conjugated polymer molecules),[40,42,43] though the presence of delayed emission reveals the contributions of bimolecular reactions involving triplets. Indeed, the ~7× faster intersystem crossing rate in TD-A compared to the pentacene dyads is largely responsible for the monomer-like EIMS response at this excitation rate.

We now consider the underlying state population dynamics over the same time scales and excitation rates presented in Fig. 2. Figure 3 displays population dynamics for the case of k_{exc} = 10^4 s^{-1} corresponding to EIMS sweeps shown in the left column of Fig. 2. Populations of singlet fission products intrinsic to each dyad model

are shown in the legend of each panel (i.e., $[T–T]^1$ or $[T–T]^5$), and explicit states considered in our model are provided as a common legend at the top ($S_1 S_1$ is a possible state, but probabilities are ~0 even at the highest excitation rate). In discussion, we will refer to $[T–T]$, which should be taken to include $[T–T]^1$ and $[T–T]^5$ where applicable. We also include the simulated $\Phi_r(k_{exc}, t)$ trends in terms of probabilities to facilitate comparison with Fig. 2.

Similar to the relatively small modulation features in corresponding EIMS responses at the same k_{exc}, state populations show relatively little change and each system spends the most time in the $S_0 S_0$ state, which is also reflected in its large occupancies (thick light-blue line). Throughout this work, the excitation rate, k_{exc}, is *per molecule*, not *per chromophore*, and via Table I, $k_{RSC} \geq 3.1 \times 10^4$ s^{-1} in the pentacene dyads; thus, this excitation regime would evince almost no modulation without the contribution of triplets produced via iSF. Importantly, $[T–T]$ states are extremely short-lived and, hence, are practically invariant over the pulse duration, also due in part to the high Prob($S_0 S_0$), which ensures the behavior at equilibrium is similar to the excitation of the relaxed system. Likewise, states with an excited singlet ($S_0 S_1$ and $S_1 T_1$) are virtually at steady state over the entire simulation for all systems. However, population dynamics of $S_0 T_1$ reveal interesting behaviors that offer useful insights of trends observed in $\Phi_r(k_{exc}, ss)$. *In particular, any large upward trend in $\Phi_r(k_{exc}, t)$ is directly correlated with* Prob($S_0 T_1$). In TD-A, the increased emission yield of $S_0 T_1$ is counterbalanced by the reduced excitation probability [we assume $\Phi_{exc}(S_0 T_1) = 1/2$], meaning the substitution of $S_0 S_0$ by $S_0 T_1$ is not apparent in the emission signal [$\Phi_r(S_0 T_1)/2 \approx \Phi_r(S_0 S_0)$]. This effect can be seen from comparing a relatively static $\Phi_r(k_{exc}, t)$ with a more dynamic Prob($S_0 T_1$) in Fig. 3(b).

Increasing k_{exc} brings about more noticeable changes in population dynamics, as also seen in fluorescence emission in Fig. 2. Figure 4 presents the case when k_{exc} = 10^6 s^{-1}, where now $S_0 S_0$ decays rapidly, and consequently, dynamics of other states become more prevalent since triplets are produced much faster than they decay. It is particularly revealing to point out trends in $S_0 T_1$ and $T_1 T_1$ states that exhibit dynamics signatures discernible over specific time regimes of the pulse duration. At early times, the $T_1 T_1$ population increases rapidly in all dyads and reaches a maximum coinciding with a large decrease in $S_0 S_0$, which also displays a characteristic "dip" and subsequent rise to steady state levels for all systems. Prob($S_0 T_1$) now evolves more slowly due to the need for one triplet to relax in order to populate this state. Comparing these state population dynamics trends to $\Phi_r(k_{exc}, t)$ also confirms that the $T_1 T_1$ growth and subsequent decay to $S_0 T_1$ dominate the behavior of this observable. Without a bimolecular process to relax $T_1 T_1$, the chromophores never get back in "sync" in the pentacene dyads, which is not the case in TD-A. Similar to lower k_{exc} values (e.g., Fig. 3), population dynamics of $[T–T]$ states are usually complete well before their $S_0 T_1$ and $T_1 T_1$ counterparts reach their steady state levels. Immediate depletion of $S_0 S_0$ means Prob($[T–T]$) is highest at the beginning of the excitation pulse and trends monotonically downwards. It also bears repeating that the simultaneous presence of two relaxed chromophores is far less probable at steady state under continuous excitation in the pentacene systems. Following this trend, but to a lesser degree, TD-A shows the highest steady state Prob($[T–T]$) due to triplet–triplet annihilation.
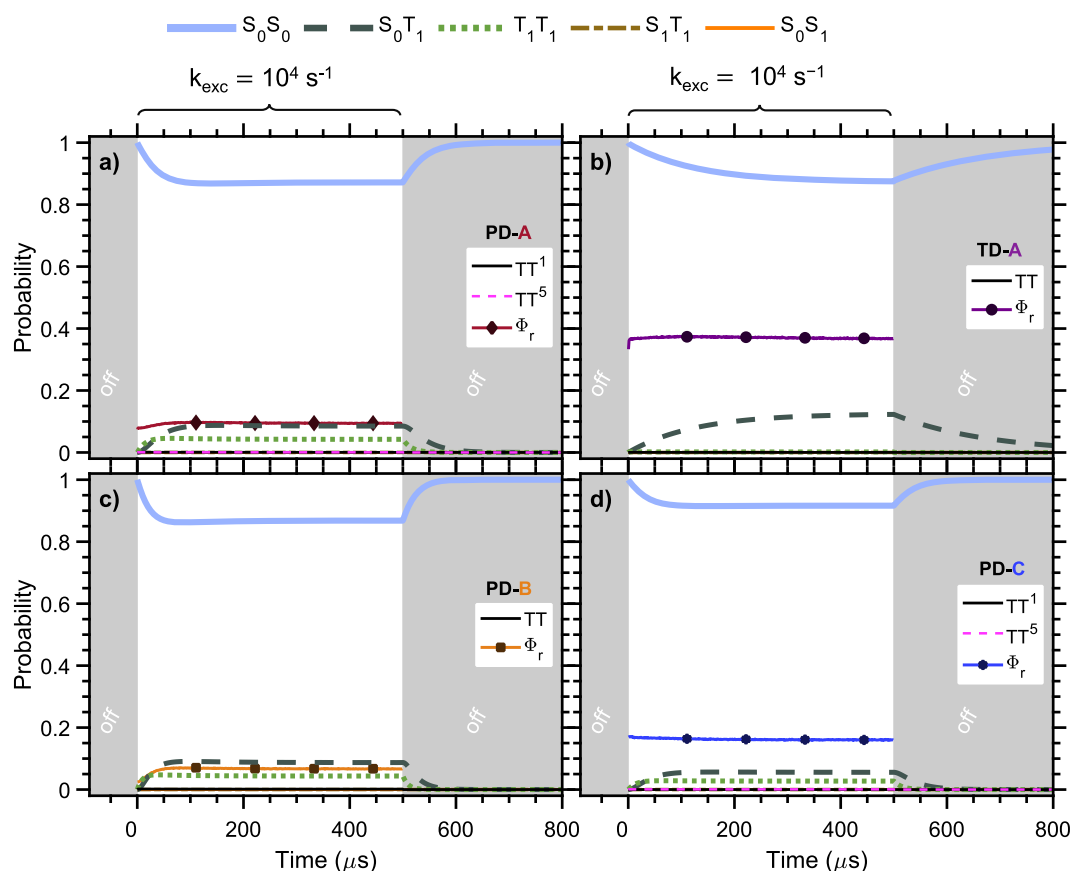
FIG. 3. State population dynamics shown as probabilities for each model iSF dyad at $k_{exc} = 10^4$ s^{-1}. A legend of states common to all models is shown at the top of the graph. Populations of model-specific states are shown in respective panels for each iSF dyad: (a) PD-A, (b) TD-A, (c) PD-B, and (d) PD-C. The fluorescence yields [$\Phi_r(k_{exc}, t)$] are displayed for comparison. Note: The relatively low k_{exc} value results in many populations overlapping at zero probability.

Figure 5 shows the case for the largest excitation rate used for our simulations ($k_{exc} = 10^8$ s^{-1}). The most striking feature of state population dynamics is the significantly faster depletion of S_0S_0 once the excitation pulse turns on. Namely, S_0S_0 reaches its steady state level at near zero probability within <1 μs, which is typically at the experimental limit of detection for EIMS.[58] This trend also explains lower initial values observed at this excitation rate [see Figs. 2(c), 2(f), 2(i), and 2(l)]; the excitation is competitive with the average excited state lifetime. Correspondingly, the singlet fission product probability, Prob([T–T]), exhibits strong and rapid growth up to a large maximum (>0.5) followed by a rapid equilibration to drastically lower steady state probabilities in the PD systems. In contrast, TD-A again demonstrates the strong effect of the triplet–triplet annihilation ($T_1T_1 \rightarrow [T$–$T]$) channel. Subsequently, Prob(T_1T_1) rises to its characteristic maximum in PD systems (which is the main cause of the emission dip) and maintains high levels at steady state. The reason why steady state populations of S_0T_1 are also substantially lower than observed for smaller k_{exc} values is that the larger excitation frequency favors greater T_1T_1 production realized through intersystem crossing from S_1T_1

to T_1T_1. Consequently, singlet fission is inhibited due to slower relaxation to S_0S_0, but Prob(T_1T_1) remains large. When excitation is ceased, relaxation dynamics of S_0T_1 show a rise in probability that coincides with the decay of the sizable T_1T_1 population. Time constants are comparable to the natural triplet lifetime ($\sim 1/k'_{ISC}$) in the pentacene-based systems, whereas triplet–triplet annihilation greatly accelerates the triplet population decay in TD-A [Fig. 5(b)].

These simulations of EIMS responses and state population dynamics illustrate several useful and practical aspects of resolving singlet fission processes on longer time scales from fluorescence emission. First, the excitation rate-dependent ground state bleach effect observed in Fig. 2 can be most readily traced to the dynamics of the states with the largest occupation probabilities, namely, Prob(S_0S_0), Prob(S_0T_1), and Prob(T_1T_1), which also correspond to the longest residence times. At low excitation rates, triplet probabilities are relatively low and population dynamics largely reflect the natural decay kinetics (i.e., k'_{ISC}). However, increasing the excitation rates effectively leads to saturation where the triplet buildup is faster, but depopulation is limited by a first order decay. The only
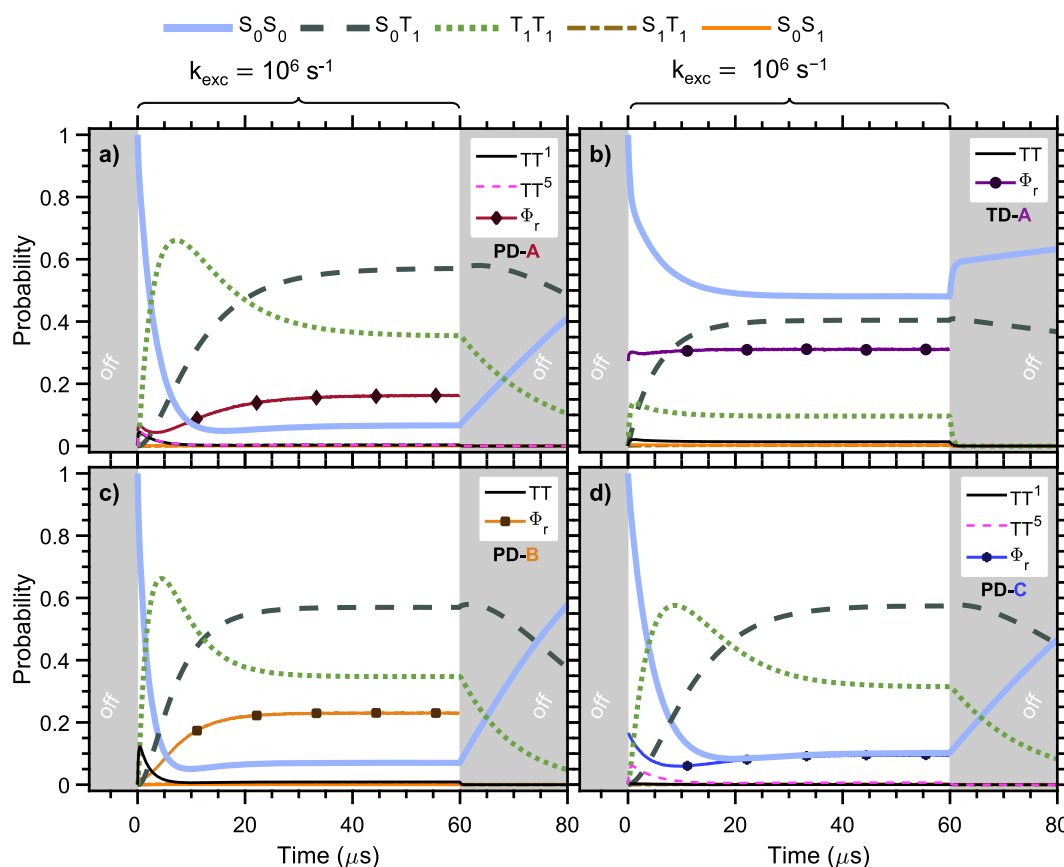
FIG. 4. State population dynamics shown as probabilities for each model iSF dyad at $k_{exc} = 10^6$ s^{-1}: (a) PD-A, (b) TD-A, (c) PD-B, and (d) PD-C. A legend of states common to all models is also shown at the top of the graph. Populations of model-specific states are shown in respective panels for each iSF dyad. The fluorescence yields [$\Phi_r(k_{exc}, t)$] are displayed for comparison.

exception to this rule is the TD-A system. Consequently, variations in $\Phi_r(k_{exc}, t)$ over the pulse duration tend to be less pronounced and increased triplet production at higher excitation rates is negated by triplet–triplet annihilation. Although it is conceivable that triplet–triplet annihilation is possible in the pentacene-based dyads, we chose to not deviate from the original models in order to ensure better harmonization of observables and populations measured from both transient absorption and fluorescence spectroscopies. For the sake of illustration, a comparison of different triplet–triplet annihilation rate constants can be found in the supplementary material; a comparatively slow triplet–triplet annihilation rate constant ($k_{TT} = 1.1 \times 10^6$ s^{-1}) has a significant effect on the EIMS response. A key objective moving forward will be to confirm that all reaction channels are valid over the entire measurement timeframe, which further requires careful control of sample conditions that are known to cause large fluctuations in responses.

Since we proposed that dips in the EIMS response are a clear indication of iSF, we now consider if the corollary is valid. In other words, is the absence of a dip proof against the operation of iSF? For the experimental parameters we used (100 ns time-bins, similar

in magnitude to commercially available multichannel analyzers), the resolution of the triplet pair state probability is not accessible, and the observable dip in the EIMS response is due to the simultaneous existence of uncorrelated triplets (T_1T_1), which prevents excitation and appears as a ground state bleach effect. Through the investigation of the TD-A system, we demonstrated that triplet–triplet annihilation can virtually erase the dip signature due to these uncorrelated triplets. Hence, in general, the corollary does not hold since the long-lived products of iSF can be eradicated by triplet–triplet annihilation, thus preventing the ground state bleach causing the dip.

However, on smaller time scales, the proposed corollary may hold. If iSF were irreversible, a dip in the EIMS response commensurate with the triplet pair lifetime would be expected but would require better time resolution. While we did not examine EIMS responses on faster time scales, such experimental capabilities do exist. However, this is predicated on the assumptions that absorption by the triplet pair state is unlikely or does not result in emission, and that the triplet pair state is slow to reform the emissive singlet.
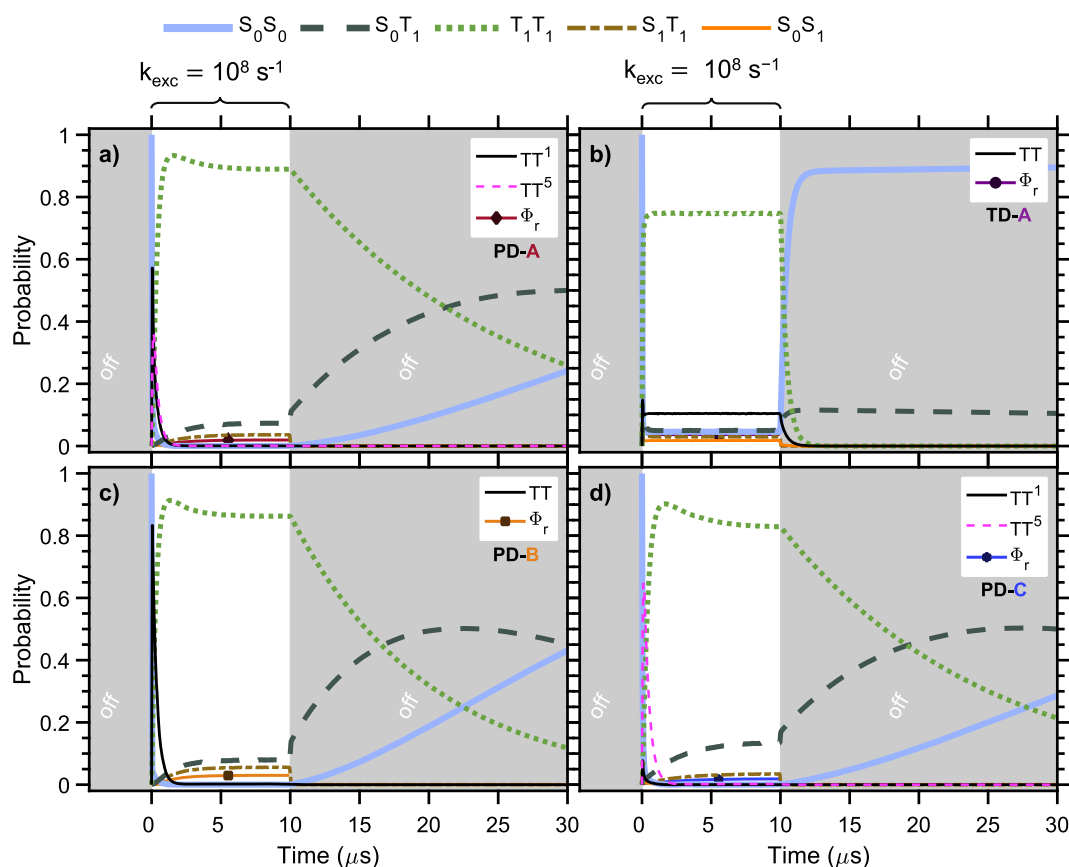
FIG. 5. State population dynamics shown as probabilities for each model iSF dyad at $k_{exc} = 10^8$ s^{-1}: (a) PD-A, (b) TD-A, (c) PD-B, and (d) PD-C. A legend of states common to all models is also shown at the top of the graph. Populations of model-specific states are shown in respective panels for each iSF dyad. The fluorescence yields $[\Phi_r(k_{exc}, t)]$ are displayed for comparison.

Based on the wealth of iSF-related behavior present in the EIMS responses above, we are optimistic that given adequate constraints, experimental data may be iteratively fit and rate constants retrieved. In this way, single molecules may be interrogated to elucidate the range of effects of conformation and nano-environment on the iSF process, with possibly paradigm-shifting outcomes. However, without sufficient fitting constraints (i.e., usage of a kinetic model and rate constant magnitudes from transient absorption spectroscopy), it may be impossible to retrieve quantitative results from an EIMS experiment.

In addition to EIMS, fluorescence correlation spectroscopies (FCS) may be used to interrogate triplet processes.[39,52,59] Unlike EIMS, which is applicable at single-molecule and ensemble levels, FCS requires the interrogation of as few molecules at a time as possible since the signal is proportional to $1/N_c$. In addition, correlation spectroscopies require excitation rates commensurate with the characteristic lifetime sought for detection, which stems from the fluorescent nature of the experiment. Specifically, if a dark period is not followed by emission, then we cannot know how long the molecule spent in a "dark" state. To investigate triplet pair lifetimes,

excitation rates of $\sim 10^8$ s^{-1} must be applied, ensuring that significant triplet populations will exist under CW excitation. Under our principal assumption that the presence of a single triplet prevents iSF in a dyad, steady state probabilities of triplet pair states in pentacene dyads under such conditions are $\sim$1% (see Fig. 5), making detection via FCS problematic. These conditions do not necessarily rule out the possibility of correlation techniques to detect singlet fission, but they do present serious obstacles for characterizing relaxed iSF systems that produce significant triplet pairs. Based on our predictions thus far, FCS may be used to access lifetimes of the T_1T_1 and S_0T_1 states. While FCS has been successfully applied to measuring triplet kinetics in three-level systems under single molecule conditions,[36,59] the more complex kinetics of iSF-active systems may be too intricate for the technique to unravel alone.

B. Tracking non-equilibrium triplet populations from temporally delayed fluorescence modulation

A variation on the EIMS experiment presented above, namely, the probing of the system with excitation light after different

periods of relaxation, is an approachable technique for estimating triplet relaxation kinetics in single molecules.[40,42,60] In contrast to the continuous excitation utilized in traditional FCS, kinetics during rest periods in variable-rest EIMS (VR-EIMS) are far more simple, which makes this method akin to transient absorption spectroscopy. In iSF dyads, the emissive response to EIMS is sometimes altogether different from the monomer [Figs. 1(b) and 2], but the principle of VR-EIMS is the same: the presence of excited states is detectable by the change in the EIMS response from that of the completely relaxed case.

Consider the response of a system that has not yet relaxed, which possessed substantial $Prob(T_1T_1)$ while at steady state conditions. During relaxation, while $k_{exc} = 0$ (i.e., when the excitation pulse turns off), T_1T_1 states decay into S_0T_1 at a rate twice that of the triplet relaxation rate constant due to the presence of two triplets that may undergo the process. Therefore, S_0T_1 is populated by T_1T_1 faster than S_0T_1 decays, assuming T_1T_1 is depleted primarily by triplet relaxation. This seemingly obvious process serves to promote $Prob(S_0T_1)$ to higher levels than possible at steady state (Fig. 5). When the system is excited with a high $Prob(S_0T_1)$, the initial emission response (I_0) will be due to a higher radiative yield than either $\Phi_r(S_0S_0)$ or $\Phi_r(k_{exc}, ss)$, the relaxed and steady state radiative yields, respectively. This result holds as long as $\Phi_r(S_0T_1) \cdot \Phi_{exc}(S_0T_1) > \Phi_r(S_0S_0)$ and is strikingly apparent in a variable-rest EIMS experiment.

In the following, we simulate VR-EIMS responses that capture each model dyad system in different stages of triplet relaxation by varying the temporal delay between successive excitation pulses. Figure 6 illustrates cases for $k_{exc} = 10^6$ s^{-1} and $k_{exc} = 10^8$ s^{-1} for each dyad with delays denoted numerically in each column. The lowest excitation rate used previously (i.e., $k_{exc} = 10^4$ s^{-1}) was not included because changes in population dynamics are too small to produce significant changes in $\Phi_r(k_{exc}, t)$. In normal EIMS experiments, delay times between successive pulses are usually made sufficiently long to ensure the system (i.e., triplets) can completely relax before the next pulse excites the molecule; here, this is only true for the first pulse in the sequence.[42]

Comparing initial Φ_r levels for each pulse offers a simple yet effective way to judge experimentally whether triplets have sufficiently relaxed. Considering the left half of Fig. 6, where $k_{exc} = 10^6$ s^{-1}, we see PD-A, TD-A, and PD-B exhibiting a similar response to shorter delay periods: The initial emission yield increases due to residual triplet populations. The opposite is true for PD-C, where shorter delay periods cause a decrease in the pulse-specific initial emission yields. TD-A again serves to contrast the effects of a radiative yield that is largely unaffected by the balance of the most emissive states: $\Phi_r(S_0T_1) \cdot \Phi_{exc}(S_0T_1)/\Phi_r(S_0S_0) \approx 1$, and the emissive response fails to reveal population dynamics. Both PD-A and PD-B show a large increase in initial per-pulse Φ_r levels (I_0) as delay times decreased indicating residual triplet populations
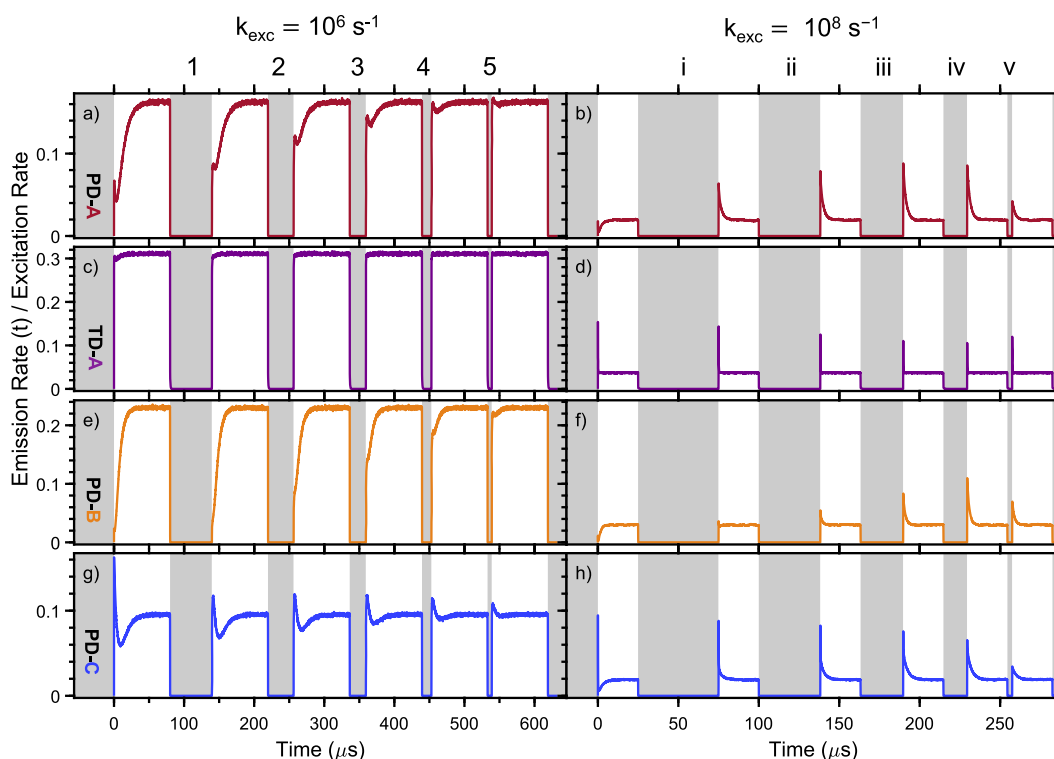

FIG. 6. Simulated VR-EIMS responses of iSF dyads depicted as fluorescence yields. Pulse delays decrease from left to right, as shown by vertical gray bars. The excitation rates are 10^6 s^{-1} (left column) and 10^8 s^{-1} (right column) for PD-A [(a) and (b), respectively], TD-A [(c) and (d), respectively], PD-B [(e) and (f), respectively], and PD-C [(g) and (h), respectively]. Delay periods for each sequence are denoted by Arabic and Roman numerals for each excitation rate, respectively.

[i.e., Prob(S_0T_1)] impeded singlet fission, hence, increased I_0. Conversely, reductions in initial per-pulse Φ_r levels were found in PD-C under the same conditions, which follows from the fact that $\frac{\Phi_r(S_0T_1)\cdot\Phi_{exc}(S_0T_1)}{\Phi_r(S_0S_0)} = 0.82$; as in a monomer, triplets in PD-C only reduce overall emission yields. Generally, when k_{exc} is equal to 10^6 s^{-1}, reducing the delay time between pulses brings initial per-pulse Φ_r levels closer to $\Phi_r(k_{exc}, ss)$ due to the inability of dyads to undergo singlet fission, while non-zero triplet populations exist. However, steady state emission counts remain nearly unchanged demonstrating that alterations in triplet production kinetics due to non-zero Prob(S_0T_1) and Prob(T_1T_1) at the beginning of the pulse do not impact population relaxation on longer time scales.

Increasing k_{exc} to 10^8 s^{-1} leads to stark changes in VR-EIMS transients due to the fact that the saturative behavior dominates for

all systems (right half of Fig. 6). Specifically, this effect appears as markedly diminished I_0 values compared to when $k_{exc} = 10^6$ s^{-1}. This saturation indicates that excitation is competitive with the decay of [$T–T$]. For the first pulse in the sequence, PD-A, PD-B, and PD-C display the usual dip feature, whereas TD-A exhibits a strong monomer-like behavior (replicating the right column of Fig. 2). As delays decrease, all dyads revert to a monomer-like behavior in terms of the shape of each emission response. TD-A shows the fastest quenching due to triplet–triplet annihilation[43] and the largest intersystem crossing yield of all the dyads. Viewing the sequence as a whole, PD-A and PD-B show initial emission levels that increase as delays decrease (maxima at pulses 4 and 3, respectively), until rest period (v), where the initial emission trend reverses. Conversely, PD-C's initial emission levels trend monotonically downward through the sequence.
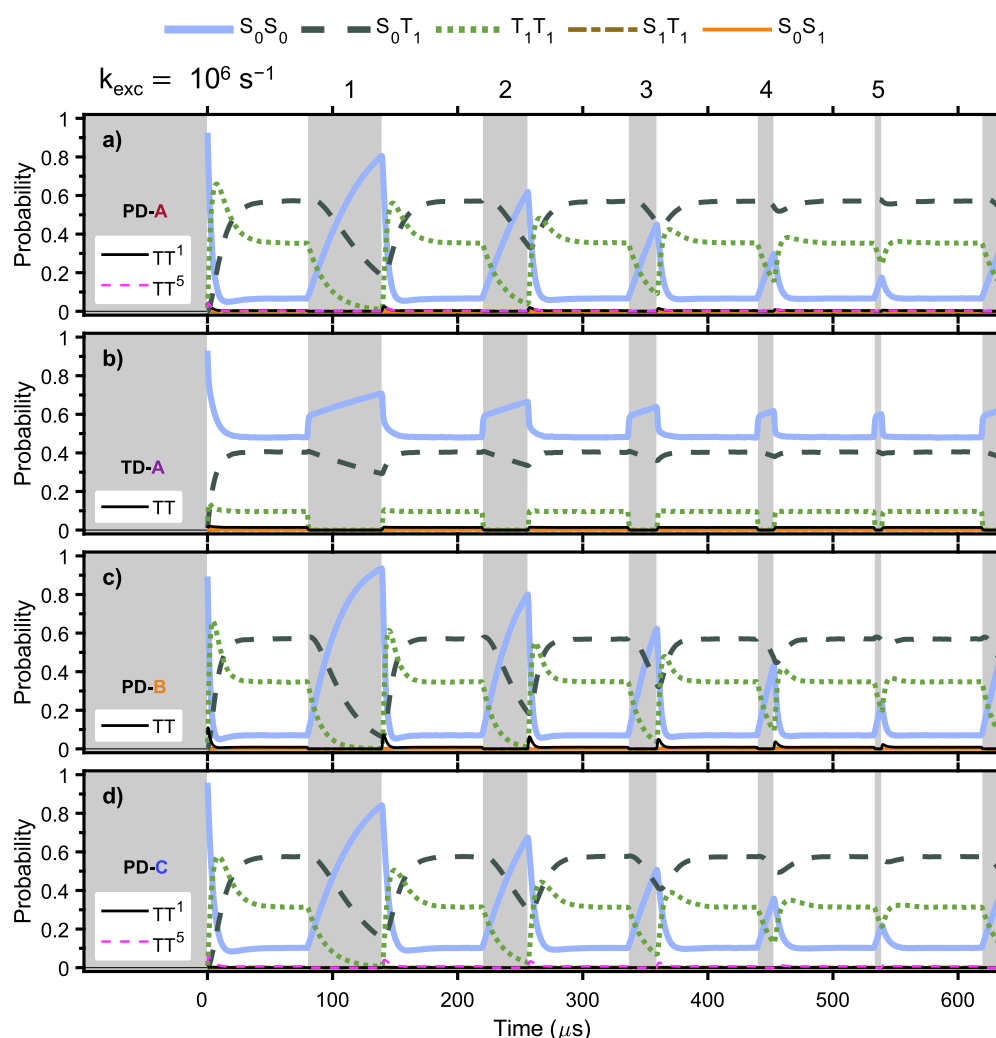

FIG. 7. State population dynamics shown as probabilities for each model iSF dyad at $k_{exc} = 10^6$ s^{-1} for VR-EIMS responses for (a) PD-A, (b) TD-A, (c) PD-B, and (d) PD-C. Similar to earlier time-dependent populations, the common states are depicted above the graph, whereas the model-specific state dynamics are shown in respective panels for each dyad.

To aid in the discussion of Fig. 6, time-dependent populations for $k_{exc} = 10^6$ s^{-1} are depicted in Fig. 7. These results illustrate how reducing the rest time between pulses causes the initial Prob(S_0T_1) to change from 0 at the start of the first pulse to approximately steady state levels at the start of the final pulse. This leads to a flattening of the EIMS response in later pulses as the initial radiative yield becomes more and more like the steady state. Meanwhile, the initial Prob(S_0S_0) changes from 1 at the start of the first pulse to near steady state levels at the beginning of later pulses, causing Prob(T_1T_1) to lose its temporary peak and thereby diminish the emission dip signature exemplified in the relaxed dyad response. PD-B shows the weakest adherence to this paradigm, mainly due to the large and fast rise in its emission yield, a characteristic resulting from the shortest transition time from TT to S_0T_1, and

largest $\Phi_r(S_0T_1) \cdot \Phi_{exc}(S_0T_1)/\Phi_r(S_0S_0)$, among all the dyads (16.6, see Table I).

Figure 8 shows the state population dynamics when $k_{exc} = 10^8$ s^{-1}, revealing that when Prob(S_0S_0) has not relaxed to 1 by the start of the excitation pulse, the ground state bleach "dip" effect in the corresponding EIMS responses is starkly reduced (compare the later pulses in the right half of Figs. 6 and 8). Moreover, we observe triplet quenching behaviors commonly observed for single emitters, as shown for the simple monomer case in Fig. 1. The inability to produce multiple triplets is due to larger Prob(S_0T_1) levels, which relax according to k_{ISC}^I. The reversion to monomer-like triplet quenching at higher excitation rates (see the right column of Fig. 6) raises intriguing questions concerning the possible interplay between states, which may be encountered in dilute solution
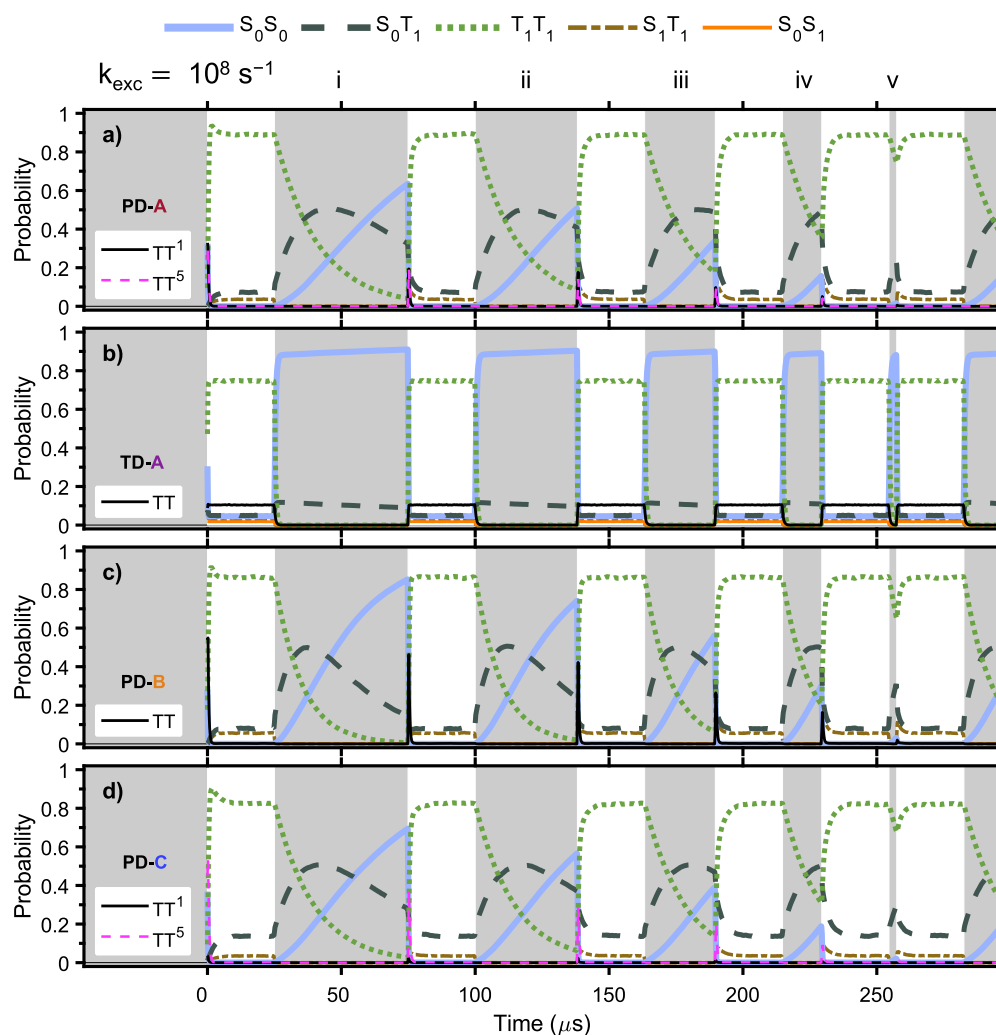

FIG. 8. State population dynamics shown as probabilities for each model iSF dyad at $k_{exc} = 10^8$ s^{-1} for VR-EIMS responses for (a) PD-A, (b) TD-A, (c) PD-B, and (d) PD-C. Similar to earlier time-dependent populations, the common states are depicted above the graph, whereas the model-specific state dynamics are shown in respective panels for each dyad.

experiments due to random orientations of active chromophores within the iSF dyad structure. Similar to Fig. 7, the possibility of triplet–triplet annihilation in TD-A leads to a rapid depopulation of $T_1 T_1$ populations resulting in relatively little change in the fluorescence yield modulation behavior with different delay times. Most importantly, the growth in initial pulse-specific emission yields at intermediate rest times [i.e., pulses iv and v in Figs. 6(b) and 6(f)] is indicative of Prob($S_0 T_1$). For instance, when triplet–triplet annihilation can be discounted, the initial emission of each pulse can be related back to the population dynamics and the triplet decay rate constant k'_{ISC}. Using a reaction rate equation, $\frac{d}{dt}[S_0 T_1] = 2 \cdot k'_{ISC}[T_1 T_1] - k'_{ISC}[S_0 T_1]$ (in the absence of excitation), which leads to a maximum in Prob($S_0 T_1$) (and thus a maximum in the initial emission yield) when $2 \cdot [T_1 T_1] = [S_0 T_1]$. This implies that the kinetics of $T_1 T_1$ and $S_0 T_1$ relaxation in productive iSF single molecules may be accessible with VR-EIMS techniques.

IV. CONCLUSIONS

Extending stochastic kinetic modeling to EIMS type experiments reveals unique dynamics signatures emerge in time-dependent fluorescence responses when iSF dyads are excited with rectangular, quasi-CW excitation waveforms. Perhaps the most notable and unambiguous emissive marker of singlet fission in dyads is the appearance of a "dip" feature from the complete ground state bleach. Population state dynamics uncover that the dip originates primarily from the formation of the relaxed and decohered triplet pair state, $T_1 T_1$. Thus, a lack of $T_1 T_1$ production or fast decay of $T_1 T_1$ will diminish the dip signature. A less robust indicator of iSF in dyads is an increase in the emission yield when excitation rates are faster than the triplet decay. This effect is peculiar because it springs from the fact that the $S_0 T_1$ state has a larger emission yield than the dyad ground electronic state, $S_0 S_0$, due to its inability to undergo singlet fission. The result is that systems that have high yields of irreversible singlet fission demonstrate rise dynamics in their EIMS response in a complete reversal of the monomer behavior. We point out that systems with low singlet fission yields (i.e., PD-C) do not show a strong dip feature or any rise dynamics, while the most productive dyad PD-B exhibits such a large dynamic increase in the emission yield that a dip is not always apparent. While only the tetracene-based iSF dyad (TD-A) included the possibility of triplet–triplet annihilation, we expect this bimolecular exciton–exciton interaction channel to play a major role in the triplet decay under excitation and in the dark. Additionally, the possibility of recycling the emissive singlet state may be realized by either the triplet pair or annihilation on longer times. VR-EIMS provides a simple way to detect triplet–triplet annihilation, especially in the case of short delay times between successive pulses. For example, if little effect on prompt intensities is observed, then abnormally shorter triplet decay times are very likely caused by triplet–triplet annihilation. VR-EIMS experiments can also directly resolve the dynamics of the $S_0 T_1$ state, which should appear as larger initial fluorescence yields within a saturative excitation regime. Overall, these simulations demonstrate that reliable correlations between multi-exciton state population dynamics and EIMS responses can be resolved in iSF dyads that enable the use of fluorescence probes to detect the singlet fission activity on time scales comparable to triplet lifetimes.

SUPPLEMENTARY MATERIAL

See the supplementary material for details of the excitation pulse generation, effects of varying intersystem crossing, triplet–triplet annihilation, and singlet fission rate constants on EIMS responses.

ACKNOWLEDGMENTS

DATA AVAILABILITY

The data that support the findings of this study are available from the corresponding author upon reasonable request.

REFERENCES

[1] M. C. Hanna and A. J. Nozik, J. Appl. Phys. **100**, 074510 (2006).

[2] B. T. Luppi, D. Majak, M. Gupta, E. Rivard, and K. Shankar, J. Mater. Chem. A **7**, 2445 (2019).

[3] A. Monguzzi, R. Tubino, S. Hoseinkhani, M. Campione, and F. Meinardi, Phys. Chem. Chem. Phys. **14**, 4322 (2012).

[4] M. B. Smith and J. Michl, Annu. Rev. Phys. Chem. **64**, 361 (2013).

[5] Y. Hong, J. Kim, W. Kim, C. Kaufmann, H. Kim, F. Würthner, and D. Kim, J. Am. Chem. Soc. **142**, 7845 (2020).

[6] J. H. Park and H. Kim, Bull. Korean Chem. Soc. **41**, 108 (2020).

[7] N. Monahan and X.-Y. Zhu, Annu. Rev. Phys. Chem. **66**, 601 (2015).

[8] A. Japahuge and T. Zeng, ChemPlusChem **83**, 146 (2018).

[9] G. D. Scholes, J. Phys. Chem. A **119**, 12699 (2015).

[10] L. Wang, Y. Wu, Y. Liu, L. Wang, J. Yao, and H. Fu, J. Chem. Phys. **151**, 124701 (2019).

[11] A. Rao, P. C. Y. Chow, S. Gélinas, C. W. Schlenker, C.-Z. Li, H.-L. Yip, A. K.-Y. Jen, D. S. Ginger, and R. H. Friend, Nature **500**, 435 (2013).

[12] R. M. Williams, H.-C. Chen, D. Di Nuzzo, S. C. J. Meskers, and R. A. J. Janssen, J. Spectrosc. **2017**, 6867507.

[13] E. C. Greyson, B. R. Stepp, X. Chen, A. F. Schwerin, I. Paci, M. B. Smith, A. Akdag, J. C. Johnson, A. J. Nozik, J. Michl, and M. A. Ratner, J. Phys. Chem. B **114**, 14223 (2010).

[14] J. Zhou and D. Jin, Nat. Photonics **12**, 378 (2018).

[15] A. B. Pun, S. N. Sanders, M. Y. Sfeir, L. M. Campos, and D. N. Congreve, Chem. Sci. **10**, 3969 (2019).

[16] Y. Y. Cheng, T. Khoury, G. C. Raphaël, M. J. Y. Tayebjee, N. J. Ekins-Daukes, M. J. Crossley, and T. W. Schmidt, Phys. Chem. Chem. Phys. **12**, 66 (2010).

[17] J. Zhao, S. Ji, and H. Guo, RSC Adv. **1**, 937 (2011).

[18] J. Hu, K. Xu, L. Shen, Q. Wu, G. He, J.-Y. Wang, J. Pei, J. Xia, and M. Y. Sfeir, Nat. Commun. **9**, 2999 (2018).

[19] J. Zirzlmeier, D. Lehnherr, P. B. Coto, E. T. Chernick, R. Casillas, B. S. Basel, M. Thoss, R. R. Tykwinski, and D. M. Guldi, Proc. Natl. Acad. Sci. U. S. A. **112**, 5325 (2015).

[20] E. Kumarasamy, S. N. Sanders, M. J. Y. Tayebjee, A. Asadpoordarvish, T. J. H. Hele, E. G. Fuemmeler, A. B. Pun, L. M. Yablon, J. Z. Low, D. W. Paley, J. C. Dean, B. Choi, G. D. Scholes, M. L. Steigerwald, N. Ananth, D. R. McCamey, M. Y. Sfeir, and L. M. Campos, J. Am. Chem. Soc. **139**, 12488 (2017).

[21] A. B. Pun, A. Asadpoordarvish, E. Kumarasamy, M. J. Y. Tayebjee, D. Niesner, D. R. McCamey, S. N. Sanders, L. M. Campos, and M. Y. Sfeir, Nat. Chem. **11**, 821 (2019).

[22] S. R. Reddy, P. B. Coto, and M. Thoss, J. Phys. Chem. Lett. **9**, 5979 (2018).

[23] R. R. Tykwinski, Acc. Chem. Res. **52**, 2056 (2019).

[24] I. Papadopoulos, J. Zirzlmeier, C. Hetzer, Y. J. Bae, M. D. Krzyaniak, M. R. Wasielewski, T. Clark, R. R. Tykwinski, and D. M. Guldi, J. Am. Chem. Soc. **141**, 6191 (2019).

[25] M. K. Gish, N. A. Pace, G. Rumbles, and J. C. Johnson, J. Phys. Chem. C **123**, 3923 (2019).

[26] T. Sakuma, H. Sakai, Y. Araki, T. Mori, T. Wada, N. V. Tkachenko, and T. Hasobe, J. Phys. Chem. A **120**, 1867 (2016).

[27] S. N. Sanders, E. Kumarasamy, A. B. Pun, M. L. Steigerwald, M. Y. Sfeir, and L. M. Campos, Chem **1**, 505 (2016).

[28] H. Liu, Z. Wang, X. Wang, L. Shen, C. Zhang, M. Xiao, and X. Li, J. Mater. Chem. **6**, 3245 (2018).

[29] N. V. Korovina, N. F. Pompetti, and J. C. Johnson, J. Chem. Phys. **152**, 040904 (2020).

[30] N. V. Korovina, J. Joy, X. Feng, C. Feltenberger, A. I. Krylov, S. E. Bradforth, and M. E. Thompson, J. Am. Chem. Soc. **140**, 10179 (2018).

[31] N. V. Korovina, S. Das, Z. Nett, X. Feng, J. Joy, R. Haiges, A. I. Krylov, S. E. Bradforth, and M. E. Thompson, J. Am. Chem. Soc. **138**, 617 (2016).

[32] D. J. Walwark, Jr. and J. K. Grey, J. Phys. Chem. A **124**, 8918 (2020).

[33] V. P. Sakun, E. M. Balashov, and A. I. Shushin, Chem. Phys. **530**, 110605 (2020).

[34] D. Dzebo, K. Börjesson, V. Gray, K. Moth-Poulsen, and B. Albinsson, J. Phys. Chem. C **120**, 23397 (2016).

[35] J. D. Cook, T. J. Carey, and N. H. Damrauer, J. Phys. Chem. A **120**, 4473 (2016).

[36] A. C. J. Brouwer, J. Köhler, A. M. van Oijen, E. J. J. Groenen, and J. Schmidt, J. Chem. Phys. **110**, 9151 (1999).

[37] A. J. Gesquiere, Y. J. Lee, J. Yu, and P. F. Barbara, J. Phys. Chem. B **109**, 12366 (2005).

[38] F. Schindler, J. M. Lupton, J. Feldmann, and U. Scherf, Adv. Mater. **16**, 653 (2004).

[39] J. Yu, R. Lammi, A. J. Gesquiere, and P. F. Barbara, J. Phys. Chem. B **109**, 10025 (2005).

[40] B. D. Datko, A. K. Thomas, Z. Fei, M. Heeney, and J. K. Grey, Phys. Chem. Chem. Phys. **19**, 28239 (2017).

[41] M. Geissbuehler, T. Spielmann, A. Formey, I. Märki, M. Leutenegger, B. Hinz, K. Johnsson, D. Van De Ville, and T. Lasser, Biophys. J. **98**, 339 (2010).

[42] A. K. Thomas, J. A. Garcia, J. Ulibarri-Sanchez, J. Gao, and J. K. Grey, ACS Nano **8**, 10559 (2014).

[43] D. J. Walwark, B. D. Datko, and J. K. Grey, J. Phys. Chem. C **124**, 13511 (2020).

[44] P. F. Barbara, Acc. Chem. Res. **38**, 503 (2005).

[45] I. Papadopoulos, Y. Gao, C. Hetzer, R. R. Tykwinski, and D. M. Guldi, ChemPhotoChem **4**, 5168 (2020).

[46] Y. Matsui, S. Kawaoka, H. Nagashima, T. Nakagawa, N. Okamura, T. Ogaki, E. Ohta, S. Akimoto, A. Sato-Tomita, S. Yagi, Y. Kobori, and H. Ikeda, J. Phys. Chem. C **123**, 18813 (2019).

[47] B. S. Basel, J. Zirzlmeier, C. Hetzer, B. T. Phelan, M. D. Krzyaniak, S. Rajagopala Reddy, P. B. Coto, N. E. Horwitz, R. M. Young, F. J. White, F. Hampel, T. Clark, M. Thoss, R. R. Tykwinski, M. R. Wasielewski, and D. M. Guldi, Nat. Commun. **8**, 15171 (2017).

[48] D. F. Anderson, J. Chem. Phys. **127**, 214107 (2007).

[49] T. Yamakado, S. Takahashi, K. Watanabe, Y. Matsumoto, A. Osuka, and S. Saito, Angew. Chem., Int. Ed. **57**, 5438 (2018).

[50] E. G. Fuemmeler, S. N. Sanders, A. B. Pun, E. Kumarasamy, T. Zeng, K. Miyata, M. L. Steigerwald, X.-Y. Zhu, M. Y. Sfeir, L. M. Campos, and N. Ananth, ACS Cent. Sci. **2**, 316 (2016).

[51] S. Lukman, A. J. Musser, K. Chen, S. Athanasopoulos, C. K. Yong, Z. Zeng, Q. Ye, C. Chi, J. M. Hodgkiss, J. Wu, R. H. Friend, and N. C. Greenham, Adv. Funct. Mater. **25**, 5452 (2015).

[52] J. Bernard, L. Fleury, H. Talon, and M. Orrit, J. Chem. Phys. **98**, 850 (1993).

[53] N. Nijegorodov, V. Ramachandran, and D. P. Winkoun, Spectrochim. Acta, Part A **53**, 1813 (1997).

[54] D. T. Gillespie, J. Phys. Chem. **81**, 2340 (1977).

[55] C. Hetzer, D. M. Guldi, and R. R. Tykwinski, Chem.-Eur. J. **24**, 8245 (2018).

[56] H. Huang, G. He, K. Xu, Q. Wu, D. Wu, M. Y. Sfeir, and J. Xia, Chem **5**, 2405 (2019).

[57] S. Ito, T. Nagami, and M. Nakano, J. Phys. Chem. A **120**, 6236 (2016).

[58] B. D. Datko, R. Grimm, D. J. Walwark, B. Burnside, and J. K. Grey, J. Chem. Phys. **151**, 044203 (2019).

[59] N. R. Verhart, P. Navarro, S. Faez, and M. Orrit, Phys. Chem. Chem. Phys. **18**, 17655 (2016).

[60] J. M. Gruber, J. Chmeliov, T. P. J. Krüger, L. Valkunas, and R. Van Grondelle, Phys. Chem. Chem. Phys. **17**, 19844 (2015).